Proceedings of the Sixth International Conference on
Railway Technology: Research, Development and Maintenance
Edited by: J. Pombo
Civil-Comp Conferences, Volume 7, Paper 3.5
Civil-Comp Press, Edinburgh, United Kingdom, 2024
ISSN: 2753-3239, doi: 10.4203/ccc.7.3.5

The Influence of Gaps Between Containers on Pressure Increase Along Freight Trains in Tunnels

J. Bell,[1] A. Henning,[1] R. Volkert,[2] O. Michael,[3] C. Renschler,[4] L. Siegel[1] and A. Buhr[1]

[1] **Institute of Aerodynamics and Flow Technology, German Aerospace Center Göttingen, Germany**
[2] **Aerodynamics and Air Conditioning, DB Systemtechnik GmbH Munich, Germany**
[3] **Technical Management Wagons, DB Cargo AG Minden, Germany**
[4] **Product Management Intermodal Sales, DB Cargo AG Mainz, Germany**

Abstract

The aerodynamic implications of freight trains travelling at operating speeds of up to 150km/h have been investigated, specifically tunnel pressure generated along the length of the train. Extensive experimental campaigns in the DLR-Göttingen moving-model facilities using reduced scale, generic freight train models and realistic loading configurations, have provided new insight into the problem. Industrial specific analysis and the subsequent results have generated recommendations for aerodynamic optimization of freight trains for high-speed operation.

Keywords: freight train, aerodynamics, tunnel pressure, experimental investigation, container, model experiment.

1 Introduction

If a train is entering, driving and exiting in a tunnel, pressure peaks are generated [1, 2, 3]. The knowledge of the pressure distribution is important in order to, for example, estimate the loads on tunnel infrastructure, on the trains themselves and on crossing trains. In order to calculate the pressure distribution and pressure wave propagation in an entire tunnel, including the reflection at the ends and the complex superpositions of the reciprocating waves, one-dimensional methods are usually used. Thereby, pressure, density and velocity in a cross section are each described by one value. Apart from the complex flow fields at the nose and tail of the train, the pressure can be approximately assumed to be constant in a cross section. Figure 1 shows the schematic illustration of the pressure development in a long tunnel after a train has entered the tunnel. The first pressure increase consists of two parts Δp_A and Δp_B. Δp_A results

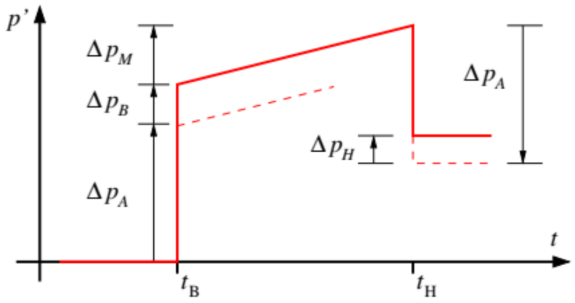

Figure 1: Schematic illustration of the pressure development in a long tunnel after a train has entered the tunnel.

purely from the displacement of the air in front of the train. The value depends on the train speed and the area ratio between train and tunnel cross-section. The flow losses, which occur in the three-dimensional flow around the train's head, cause the additional pressure increase Δp_B. These are realized in the one-dimensional modeling by additional friction in the head section. The coefficient is adjusted accordingly so that the same pressure increase Δp_B results in the simulation. At time t_H the rear of the train reaches the observer. In the meantime, the pressure has continuously increased by Δp_M due to surface friction along the train. The friction coefficient of the 1D model is chosen so that Δp_M from the simulation matches the observed increase. The train's wake would decrease the pressure again by Δp_A without any losses in the tail region. The pressure drop observed at t_H is reduced by the pressure losses in the flow around the tail Δp_H. By adjusting friction coefficient in the train rear section, the simulated pressure reduction can be adapted to the measured one. In principle, the friction on the tunnel wall is also responsible for the pressure increase Δp_M and the increase also depends on the friction coefficient reflecting turbulence, which in most cases simply set to an empirical value that fits the particular tunnel. The tunnel in the DLR-Göttingen moving-model facility (TSG) is 16 m long and the model has a length of 2.7 m [5]. This boundary conditions of the tunnel test facility do not allow the afore-

mentioned pressure increase in the tunnel to be recorded after the train has entered the tunnel completely. The distance at which the train is completely entered the tunnel is too short to observe the phenomenon clearly. The reason for this is the pressure wave caused by the train entering the tunnel, which accelerates in front of the model, then reflected at the end of the tunnel and travels back through the tunnel against the train direction. There it meets the moving train and dominates the pressure distribution in the tunnel. The pressure increase caused by the train's enlarging boundary layer is then superimposed by this wave traveling through the tunnel. A pressure sensor mounted in the tunnel then measures the cumulative effects of the pressure wave and boundary layer effects as the train passes; differentiation between the effects is not possible in post-processing. A novel technique to obtain meaningful results on the pressure increase in the tunnel is the measurement of differential pressure directly on the train model surface. For this purpose, one pressure sensor is placed upstream and one downstream of the center variable test-section of the model. Both sensors then measure pressure fluctuations, which are also affected by the pressure wave reflection phenomenon described above. However, both sensors experience the same amplitude triggered by the pressure wave. If the difference from both signals is measured, the pressure difference remains, which is caused by the enlarged boundary layer of the train. This enables the investigation of the influence of different configuration on the pressure gradient in the tunnel.

2 Experimental Setup

The experimental investigation has been performed in the DLR-Göttingen moving-model facility (TSG). In this experiment, a $1:22.7$ reduced scale generic freight train model is accelerated by a catapult mechanism up to $45\,\mathrm{m/s}$ $(160\,\mathrm{km/h})$. The model then coasts freely on functioning bogies across a rail, through a $23\,\mathrm{m}$ long test-section where measurements are made. After travelling $60\,\mathrm{m}$, the model is decelerated in a braking tank filled with polystyrene balls. For further information about the facility, see [5].

The test-section of the moving-model facility was configured to perform the tunnel pressure experiment. A $16\,\mathrm{m}$ long, $0.07\,\mathrm{m}^2$ cross-sectional area tunnel (corresponding to $36\,\mathrm{m}^2$ in full scale) was installed on the $19\,\mathrm{m}$ long plate. A flat ground was installed, to which the tunnel sides fit into. The tunnel started $2.4\,\mathrm{m}$ from the start of the flat $1.12\,\mathrm{m}$ wide test-section plate, and ended $1\,\mathrm{m}$ prior to the end of the flat plate - this ensured flow into and out of the tunnel was representative of real-world operation. The tunnel test-section configuration is illustrated in Figure 2, with photos in Figure 3. A $1:22.7$ scale, $2.7\,\mathrm{m}$ long, $0.0182\,\mathrm{m}^2$ cross section (corresponding to $61.3\,\mathrm{m}$ long, $9.115\,\mathrm{m}^2$) generic freight train was used in the experiments. In addition the moving model had a section where surface roughness elements can be applied, to increase the surface boundary layer, and artificially simulate a longer train, upstream of the model test-section. The mounted spire elements are had a height of $10\,\mathrm{mm}$, width of $16\,\mathrm{mm}$, and spacing of $16\,\mathrm{mm}$. The spires were applied at 6 stages starting $120\,\mathrm{mm}$ from the

nose. After the spires, 250 mm length of Lego base plates was applied, which has generic roughness of 5 mm diameter, 1.5 mm cylinders with 3.5 mm spacing.

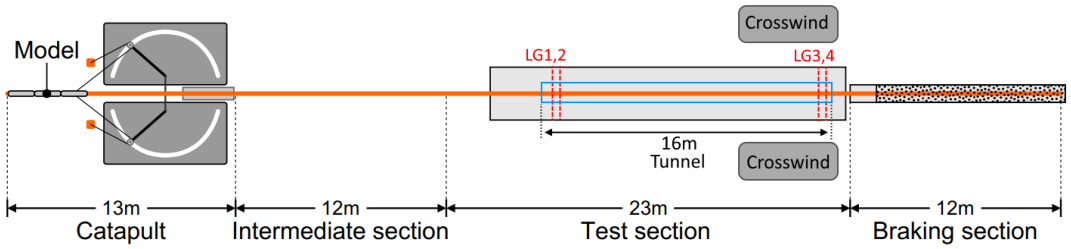

Figure 2: TSG (Tunnel-Simulation facility Göttingen) moving-model facility diagram in tunnel pressure measurement configuration

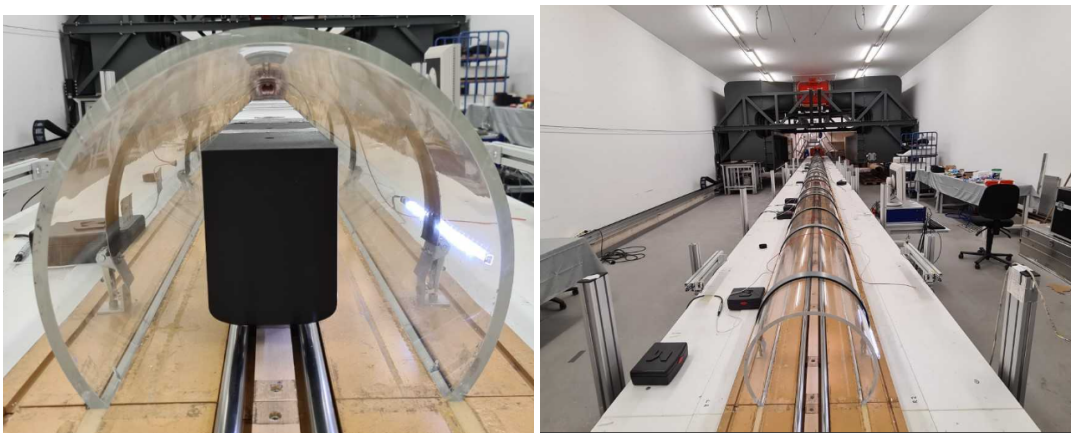

Figure 3: left: Tunnel and moving-model in moving-model facility. right: Tunnel and wall-mounted pressure sensors in moving-model facility

3 Measurements

The primary measurements in the tunnel pressure experiment were differential pressure, Δp, measurements on the trains surface. The difference in pressure, Δp, between the front, p_1, and behind, p_2, the test-section are of focus in this experiment. Pressure taps (0.5 mm holes on the surface) are located on each side of the nose section, at $z = 62$ mm and $x_1 = 0.925$ m (100 mm from the end of the nose upstream dummy). The two taps were connected to a pressure manifold and connected to one side of a pressure transducer. There were two additional pressure taps at $x_2 = 2.382$ m on the downstream dummy, at the same height of $z = 62$ mm. These were also connected to a manifold, and then connected to the other side of the pressure sensor. The manifold effectively creates a passive average of the pressure measured at both sides, reducing

any local fluctuations, which are not of interest in this experiment. The pressure sensor then directly measures the pressure change across the test-section, generated by the different realistic loading configurations tested. The distance between the upstream and downstream taps was $1.457\,\mathrm{m}$ (see Figure 4), which corresponds to $33.07\,\mathrm{m}$ in

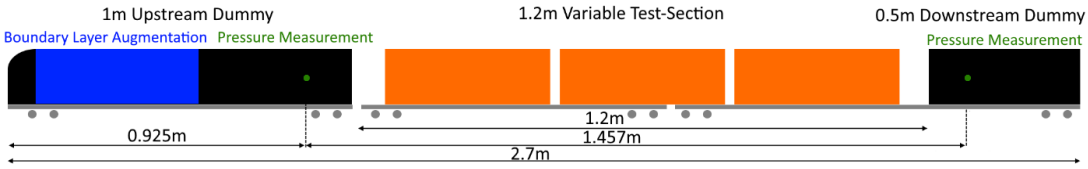

Figure 4: Generic $1:22.7$ scale freight-train moving-model in surface-pressure measurement configuration

full-scale. The pressure difference measured, across this distance, can be referred to the pressure gradient.

The pressure sensor was located in one of the containers in the test-section, and was connected to an on-board data acquisition system. An accelerometer, and a light sensor were also connected, and 3 second samples were taken at $5000\,\mathrm{Hz}$ with this system. 2 light gate pairs measured the model velocity, and atmospheric pressure sensor and temperature sensor were used to determine the air density.

Secondary pressure measurements were also obtained using 9 pressure sensors installed in the tunnel wall at a height of $z = 50\,\mathrm{mm}$, and longitudinal positions of: $x = 0.62, 2.98, 4.99$ (both left- and right-hand sides), $7.35, 8.35, 9.0, 9.05, 9.99\,\mathrm{m}$. These measurements were used to validate the data sanity of the pressure measured from the on-board data acquisition system. The transient pressure measured from these tunnel wall mounted sensors is highly sensitive to the pressure wave that is generated as the train nose enters the tunnel, which accelerates in front of the model and reflects back once it reaches the tunnel exits. This means the wall measurements measure both the train tunnel pressure, and the reflections, making it difficult to isolate the pressure gradient that occurs along the train as it passes the sensor. In contrast, the pressure gradient is measured directly with the on-board sensor, and this time signal can be averaged whilst it passes through the tunnel, in an attempt to remove the effects of any pressure wave reflections.

4 Results

4.1 On-board-Measurements

An example of the data acquired during one measurement 'run' of the moving-model passing through the tunnel is presented in Figure 5. The transient signals from the pressure transducer, accelerometer and light sensors are illustrated. The pressure is the primary data for the experiment. The accelerometer is used to trigger the measurement

(once the model starts moving) and to confirm vibrations during movement across the rails isn't significantly affecting the pressure sensors. The light sensor is used to spatially locate the model, and provide a secondary model velocity location. Visible in

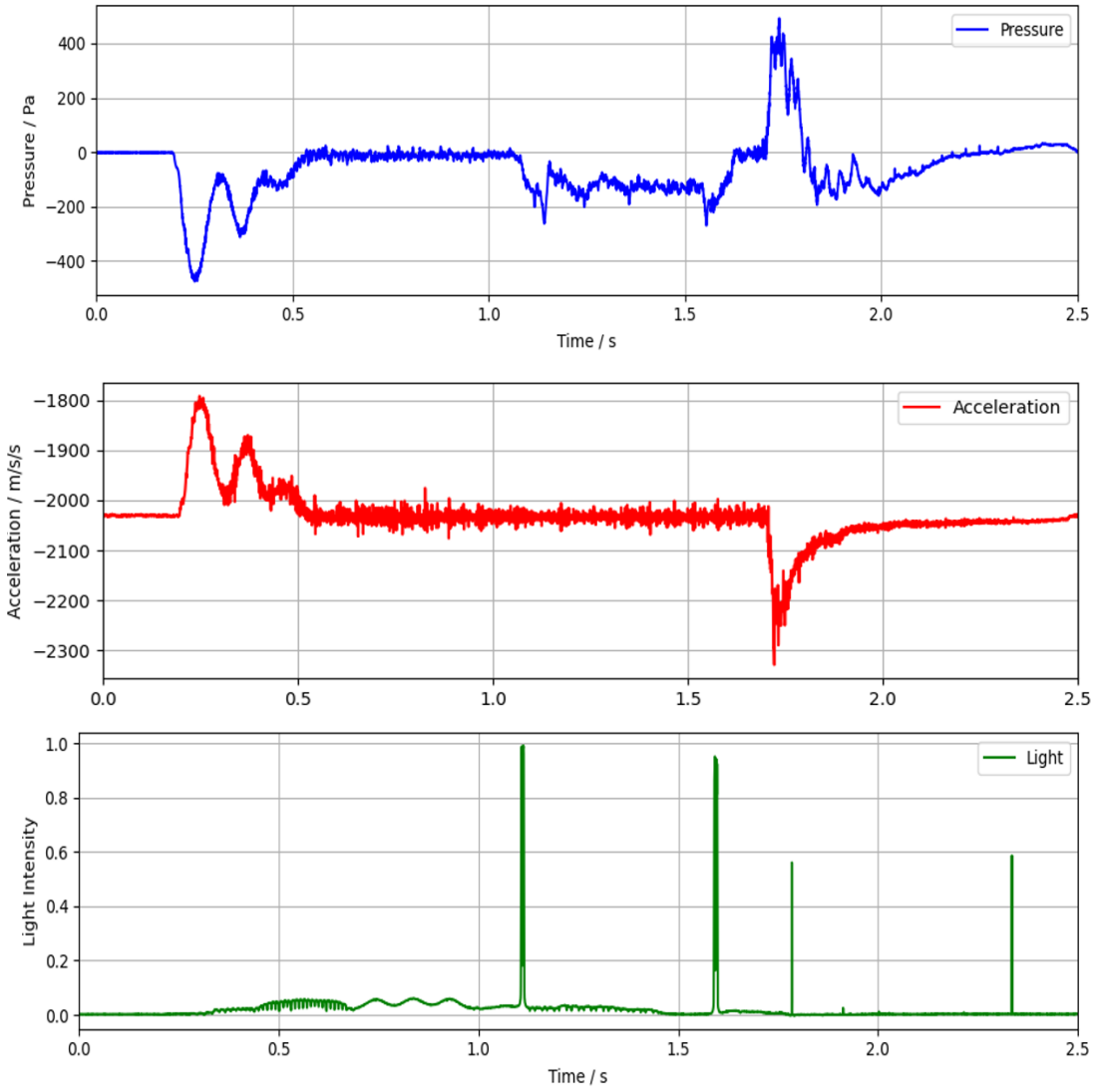

Figure 5: Example data from on-board data acquisition system: transient pressure, acceleration and light signals

the pressure and accelerometer signals is a triple-peaked wave signal at the start from $0.2 - 0.6$ seconds. This is the signature of the strong acceleration the model experiences as it is moved from stationary to the test-velocity of $> 32\,\text{m/s}$ ($> 110\,\text{km/h}$) in the space of a few meters. The wavy nature is a feature of the accelerating pneumatic arms that pull the rope, which in turn accelerates the model. This characteristic is visible in both accelerometer and pressure signals, as the acceleration is so high, that it affects the pressure diaphragm in the pressure sensor. However, the pressure at

this point of time is not of interest for this investigation. After this time, at $0.6 - 1.0$ seconds, the model moves freely across the rails, and then at $\sim 1.2 - 1.6$ seconds passes through the tunnel, before entering the brake tank at ~ 1.75 seconds. Prior to entering the tunnel the pressure signal shows relatively consistent level of ~ 0 Pa, with minor fluctuations. Strong peak and pressure fluctuations occur in during tunnel entry and exit, with a relatively stable level within the tunnel, with minor waves visible. In contrast, the accelerometer signal shows no clear sign or fluctuations before or during the tunnel passing. Thus, although at the start of the test, it is demonstrated that the pressure sensor is capable of being affected by accelerations/vibrations, the area of interest, during tunnel passage, is not expected to have any significant impacts from vibrations, any pressure signals measured can be attributed to aerodynamics.
The light signal shows two clear peaks at ~ 1.2 and 1.6 seconds, associated to the light gates mounted in the side walls of the tunnel. These peaks are used to spatially locate the tunnel start and end in the on-board data acquisition system measurements, enabling the pressure signal to be associated directly to tunnel the influence of the tunnel. Additionally, the two light gates, with a known distance between them in the test-section, and subsequent known time-lag between the two peaks in the light sensor, enables an additional model velocity calculation to be performed and validate the trackside light-gates utilized in the moving-model facility as the primary model velocity measurement.

4.2 Surface-Pressure Measurements

In Figure 6, the pressure signal for four individual runs with the same test conditions are presented. The figure demonstrates that for the same smooth loading configuration, and same test velocity of 32 m/s the transient pressure signal is remarkably consistent. Once the model is moving freely in the test-section, both in open air ($0.5 - 1.2$ s) and through the tunnel ($1.2 - 1.6$ s), the flow around the model is highly turbulent, and thus the pressure on the surface fluctuates, and thus transient signals are not expected to be exactly the same (fluctuations can occur at different times). This is visible in the results, but the main features, average pressure signals, and tunnel specific features are very consistent between the four individual runs. This is illustrated more clearly in Figure 7, where a zoom in of the tunnel section is plotted.

In Figure 7, pressure is presented as the pressure coefficient C_p:

$$C_p = \frac{\Delta p}{q}, \tag{1}$$

where Δp is the difference in pressure measured at the front and rear of the model (either end of the model's variable test-section), $\Delta p = p_{front} - p_{rear}$, and this pressure is normalized by q, which is the dynamic pressure the model experiences as it moves through the air. In this case, the dynamic pressure q is calculated as:

$$q = 0.5 \rho V_T \tag{2}$$

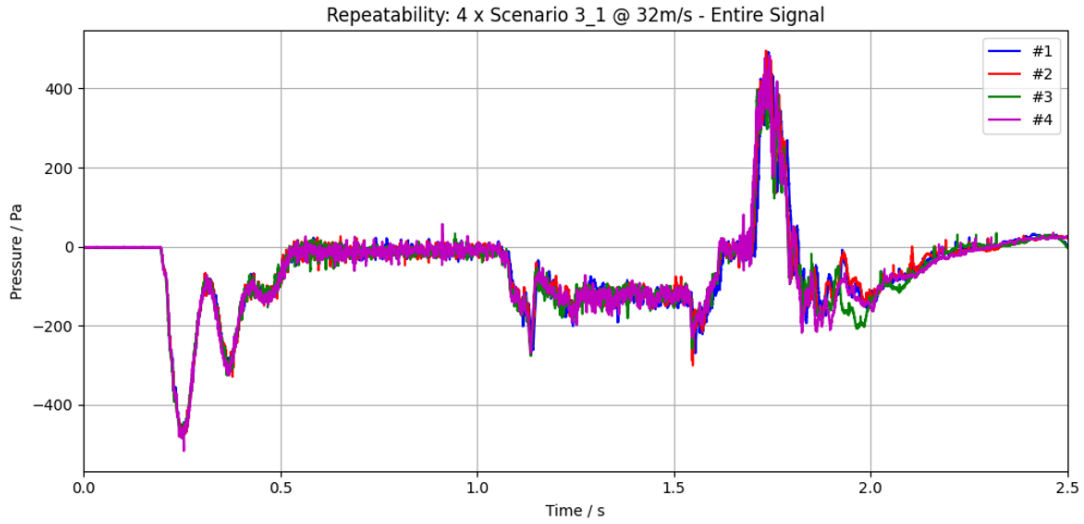

Figure 6: Transient pressure signals for 4 repeated 'runs' at the same 32 m/s model speed

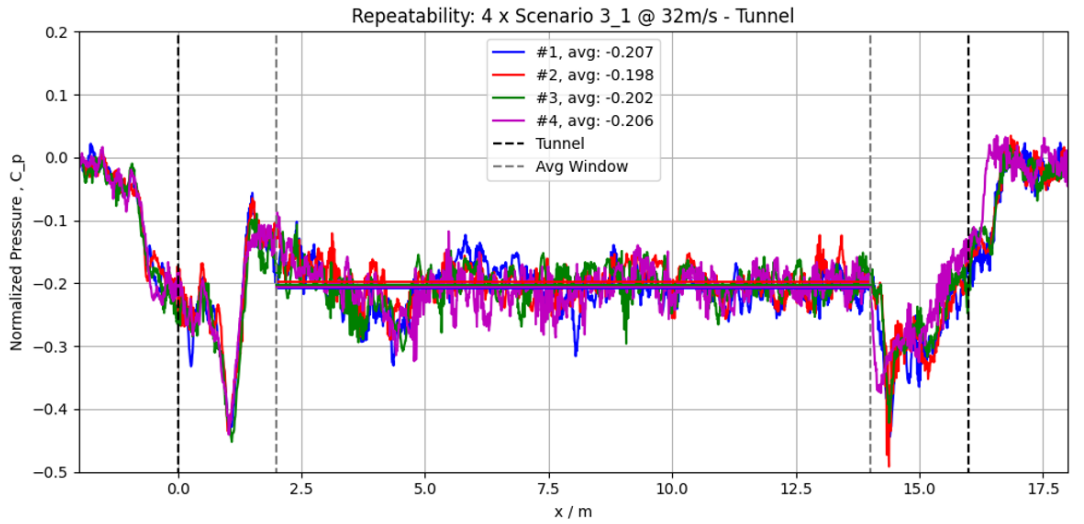

Figure 7: Pressure during tunnel passage for 4 repeated 'runs' at the same 32 m/s model speed.

where V_T is the model speed determined by the light gates, and the density ρ is determined from the ideal gas equation and the measured temperature and barometric pressure in the facility test-section. This allows the pressure results from different test velocities (from Reynolds number sensitivity tests, and even slightly different test speeds run-run) to be directly compared to each other, as the pressure magnitude is no longer directly related to velocity.
Additionally, in Figure 7, the normalized pressure C_P is plotted in space (x/m), rather

than time (t/s). The model speed V_T was used to convert from the temporal to the spatial domain. This enables plotting of the pressure, directly related to the location of the tunnel. The data is then and aligned with the location of the tunnel, with $x = 0$ at the tunnel start. All further results will be presented in this manner.
The mean pressure between 2 and $14\,\mathrm{m}$, of the $16\,\mathrm{m}$ long tunnel was also calculated for each run, and is included in the plotted results in both the legend, and as a solid horizontal line (plotted between $x = 2 - 14\,\mathrm{m}$). This value is used to assess the overall tunnel pressure performance of each loading configuration. The average window is large enough for small, turbulent fluctuations not to have a significant impact, and also includes multiple of the visible waves from the pressure reflections. This is representative of the average increase in pressure the specific loading configuration generates across the modelled length.
Therefore, with this improved processing and plotting in Figure 7, different minor fluctuations are visible, but the key peaks and troughs during tunnel entry and exit are very consistent across the four runs. Similarly, the slight wave within the tunnel passage between the tunnel entry and exit is consistent, this is due to the reflection of pressure waves generated at the nose, and reflected at the tunnel exit. Importantly, the average pressure within the tunnel is also very consistent, where the average normalized pressure is $0.198 - 0.207$. This high level of repeatability of the results enabled confidence in the results, as well as informed the test procedure, where 2 measurements of each test-configuration was performed.
The same smooth loading configuration (3_1) was tested, in this case with an augmented boundary layer as described in section 2, for four different model velocities, to assess for Reynolds number sensitivity. The transient pressure during the tunnel passage is presented in Figure 8 for model velocities of 32.0, 33.9, 37.3 and $40.5\,\mathrm{m/s}$. This corresponds to Reynolds numbers, with width as the characteristic length, of Re_W = 2.40×10^5, 2.55×10^5, 2.80×10^5, 3.0×10^5. Similarly to the repeatability results, the pressure signals are remarkably consistent for the four different runs. The only feature that is observably different, is the peak after tunnel entry at $2.5\,\mathrm{m}$. This can be attributed to the pressure wave reflection, and thus the difference is related to the difference in model speed, as it reaches the reflection at different times/space. The pressure of interest, the mean pressure during the tunnel passage is consistent for the different test speeds, thus the results are Reynolds number insensitive, and thus able to be applied to full-scale (larger Reynolds number) for interpretation.

4.3 The Effect of Loading Configuration

The transient pressure signals during tunnel passage for six different loading configurations (illustrated in Figure 9) are presented in Figure 10. In addition to the 5 realistic loading configurations: three ‘smooth’ and two ‘rough’ configurations, a ‘Closed’ configuration was also tested, where no gaps of any size were included in the model, it was a constant cross-section. The closed configuration provides a reference point to compare the other configurations to. Figure 10 presents the same results, with a $0.1\,\mathrm{m}$ moving average applied to the pressure profiles, to allow clearer comparisons to be

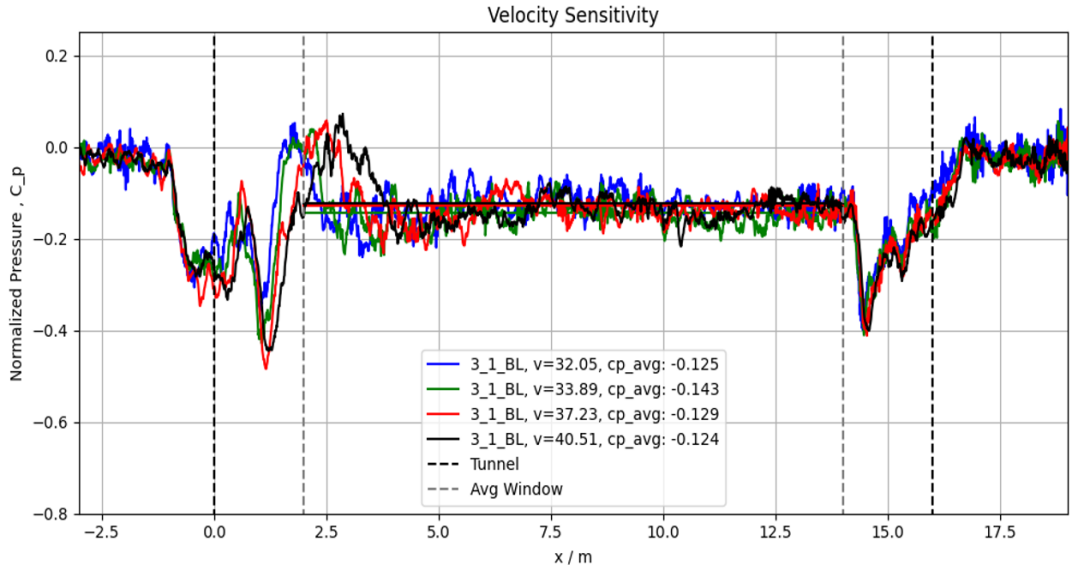

Figure 8: Pressure during tunnel passage for 4 different model speeds 32, 33.9, 37.2 and 40.5 m/s.

made. Both figures show the mean pressure in the legend and as horizontal lines. Figure 11, the mean pressure is also presented as a bar graph for more direct comparison.

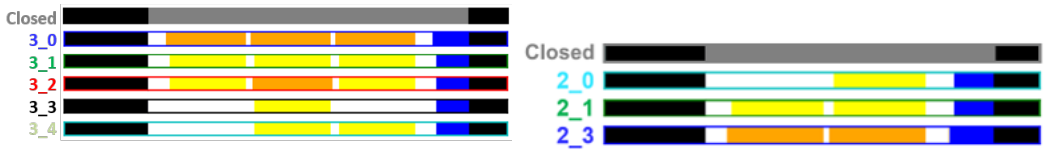

Figure 9: Graphical representation of loading configurations on 80 ft. wagon (left) and 52 ft. wagon (right). Representative of 'realistic' operational configurations based on WK7,3 (yellow) and WK7,7 (orange) swap body containers (7.45 and 7.82m long respectively)

The results show that the tunnel pressure generated along the length of the train is highly sensitive to loading configuration. Rough configurations with large, container sized gaps, have likewise significant increases on the pressure ($C_P = 0.291 - 0.385$), compared to smooth configurations with only medium and small gaps ($C_P = 0.114 - 0.207$). The size of the medium wagon-wagon gap also has a non-negligible effect, where the difference between 3_0 (1.4 m gap in full scale) and 3_1 & 3_2 (1.8 m gap) configurations is $C_P = 0.114$ and $0.207, 0.206$ respectively. Whilst differences in small, container-container gaps on the same wagon ($0.6 - 0.8$ m in full scale), has negligible impact, as the 3_1 and 3_2 pressure results are basically the same. Additionally, the best-case smooth configuration of 3_0 is shown to have very good tunnel

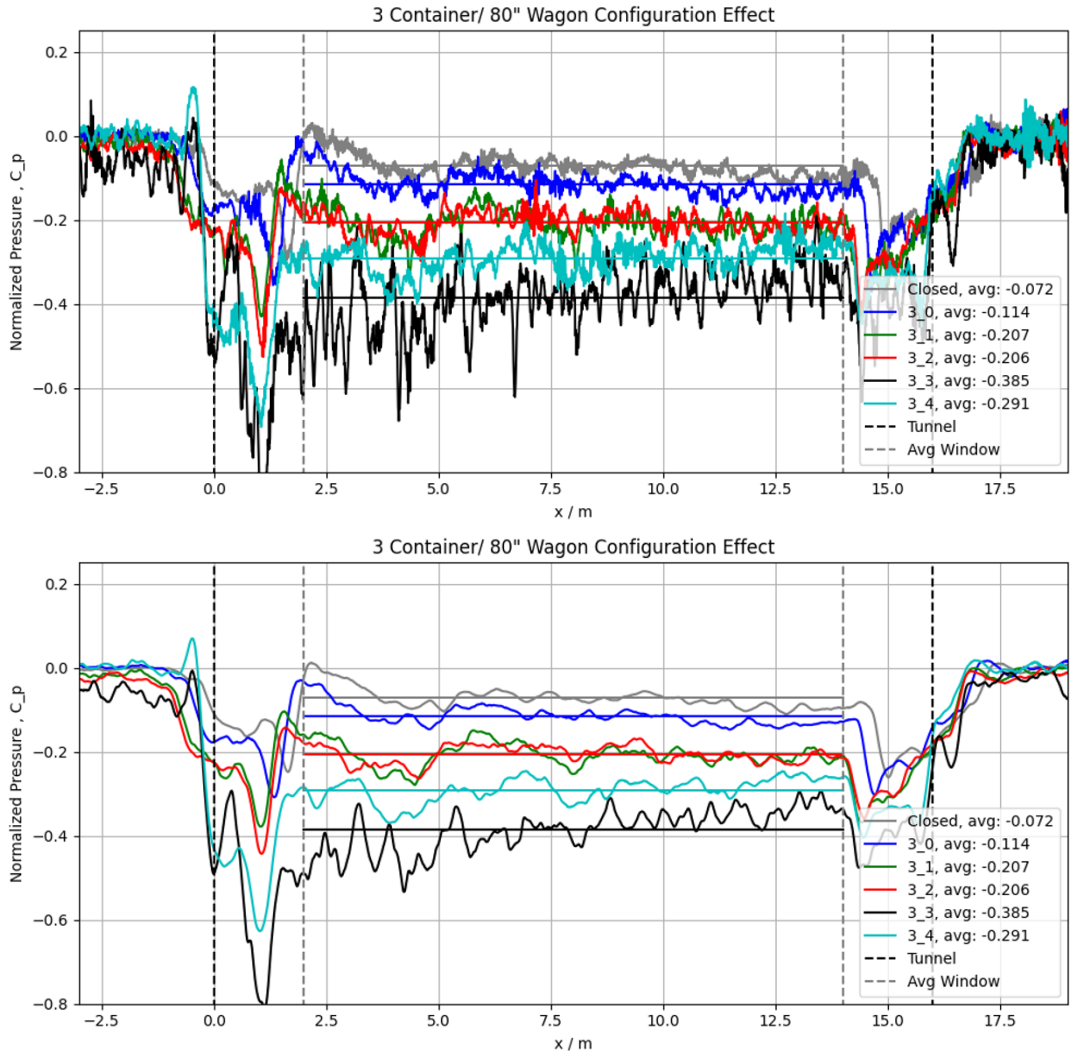

Figure 10: Pressure during tunnel passage for different 80 ft. wagon loading configurations, raw data (upper) and filtered data (lower).

pressure performance, not much worse than the fully closed reference configuration. The relative change in pressure between different configurations of $C_P \approx 0.05 - 0.1$ is significantly larger than the run-run repeatability variation of $C_P \approx 0.01$, providing confidence in the results.

The same trends are visible in 3 realistic loading configurations on a 52 ft. double wagon (illustrated in Figure 9), presented in Figure 12. The large container sized gap in configuration 2_0, has a significantly greater pressure change across the test-section, relative to the two smoother configurations 2_1 and 2_3. The colours each of these configurations are the same as the respective similar loading configurations of the 80 ft. triple container loading configuration. Again, similarly to the 80 ft. pressure results, large gaps have the most significant impact, C_P increases from ≈ 0.1 to 0.259. The medium wagon-wagon gap distance also has a non-negligible effect: the pressure

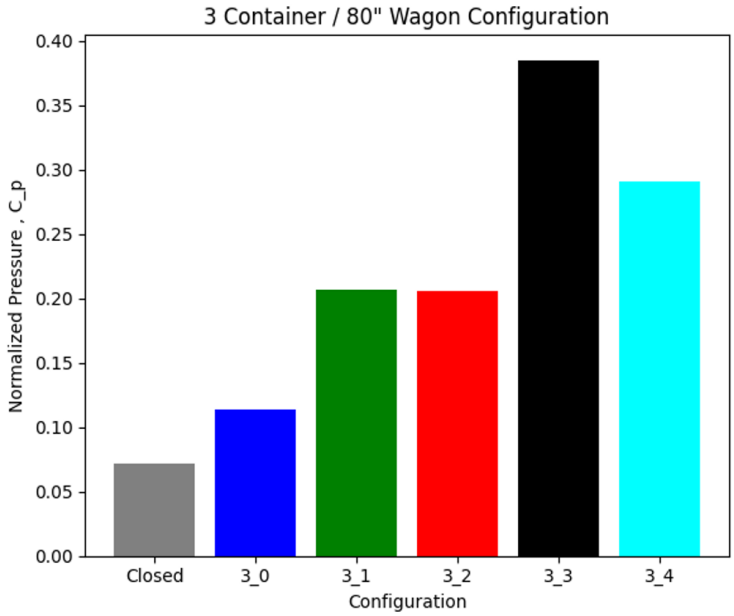

Figure 11: Average pressure during tunnel passage for different loading configurations.

generated by configuration 2_1 is 0.115, an increase over 0.091 of configuration 2_3. Whilst this 'smoothest' realistic loading configuration of 2_3, with the smallest gaps overall, compares well to the fully closed (no gaps) configuration which has a pressure level of 0.072.

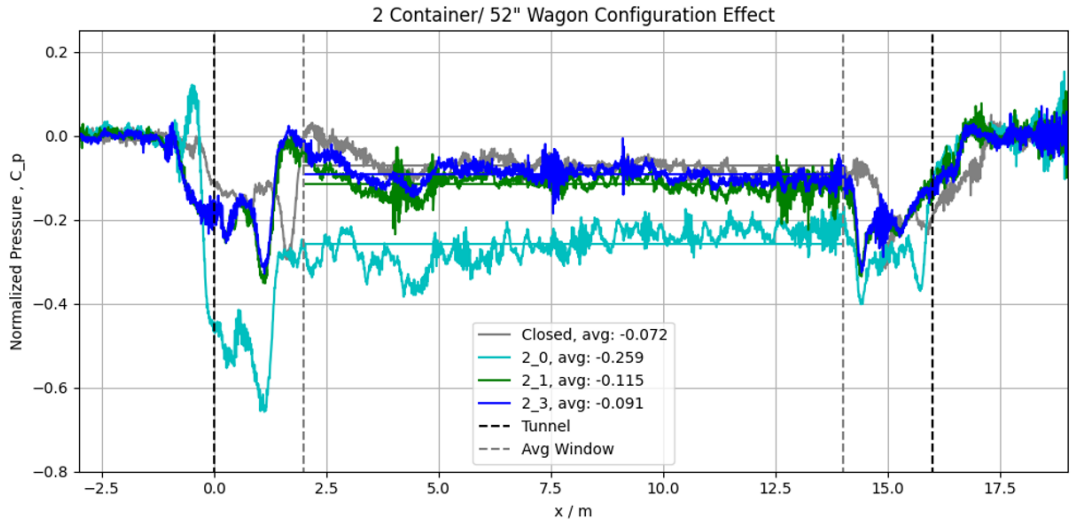

Figure 12: Pressure during tunnel passage for different 52 ft. wagon loading configurations.

5 Conclusion

The direct measurement of change in pressure before and after the realistic loading configuration section of the model functions successfully, with repeatable results, and significant variation of the results between loading configurations. The effect of loading configuration on tunnel pressure can be sumarized as the following. Strong effect can be observed in case of large, container-sized gaps, weak effects effects in case of wagon-wagon container gaps and negligible effect for inter-container gaps. Both the 80 ft. and 52 ft. wagons demonstrate the same trends, no significant difference in the results are apparent. Indirectly from these results, is the finding that 80 ft. (triple container) wagons are more beneficial than 52 ft. (double wagons) for optimized tunnel pressure, as they result in fewer medium wagon-wagon gaps for the same given train length.

References

[1] Heine, D., Ehrenfried, K. (2014). Experimental Study of the Pressure Rise due to Tunnel Entry of a High-Speed Train. In: Dillmann, A., Heller, G., Krämer, E., Kreplin, HP., Nitsche, W., Rist, U. (eds) New Results in Numerical and Experimental Fluid Mechanics IX. Notes on Numerical Fluid Mechanics and Multidisciplinary Design, vol 124. Springer, Cham.

[2] D. Heine, K. Ehrenfried, G. Heine, S. Huntgeburth (2018). Experimental and theoretical study of the pressure wave generation in railway tunnels with vented tunnel portals, Journal of Wind Engineering and Industrial Aerodynamics, Volume 176, 2018, Pages 290-300, ISSN 0167-6105.

[3] Baker, C. J. "A review of train aerodynamics Part 1–Fundamentals." The Aeronautical Journal 118.1201 (2014): 201-228.

[4] Tomoshige HARA, Aerodynamic Force Acting on a High Speed Train at Tunnel Entrance, Bulletin of JSME, 1961, Volume 4, Issue 15, Pages 547-553, Released on J-STAGE February 15, 2008, Online ISSN 1881-1426, Print ISSN 0021-3764

[5] D. Heine, K. Ehrenfried, G. Heine, S. Huntgeburth (2018), Experimental and theoretical study of the pressure wave generation in railway tunnels with vented tunnel portals, Journal of Wind Engineering and Industrial Aerodynamics, Volume 176, Pages 290-300, ISSN 0167-6105.